



Stochastic and Non-linear effects in Biological Systems

Memoria de investigación presentada por Niko Komin, en el Departamento de Física de la UIB, el 22 de octubre 2008.

Esta memoria de investigación ha sido dirigida por el Doctor *Raúl Torral* del Departamento de Física de la UIB.

Electronic version is available at <http://ifisc.uib.es/publications/>

Printed 22nd of October 2008.

Contents

Preface	1
1 Introduction	3
1.1 Motion in biology as a dynamical system	3
1.1.1 Random walkers	4
1.1.2 Active Brownian particles	6
1.2 Biochemical and biophysical reactions	7
1.2.1 Simple enzyme reactions	7
1.3 Drug absorption	8
1.3.1 Compartment models	10
1.3.2 Multi Drug Resistance (MDR) transporter	11
1.4 Outline	12
2 The Daphnia	13
2.1 Daphnia as random walkers	14
2.1.1 Two angles	16
2.1.2 Gaussian distribution	16
2.2 A food model	17
3 A Three-Compartment Model	19
3.1 Model and method	19
3.1.1 Potential and friction	20
3.1.2 An approximated solution	21
3.2 Michaelis-Menten type flux	23
3.2.1 Method application	24
3.2.2 Comparison with experiment	25
3.2.3 Parameter dependence	28
3.2.4 Error propagation	29
3.3 Other nonlinearities and extensions of the model	31
3.3.1 Michaelis-Menten with cellular retention	32
3.3.2 Outlook	32
4 Conclusions	35

Bibliography	41
Curriculum Vitae	i

Preface

In 1827 Robert Brown discovered the erratic movement of small particles in a liquid. As a botanist he considered a biological reason for it but about 80 years later Einstein [1] and Smoluchowski [2] explained the effect as the result of many erratic collisions with the liquid's molecules due to the thermal movement.

Applying mathematical models to true biological effects goes back to about the same time. In 1906 Pearson and Blakeman wrote *Mathematical contributions to the theory of evolution* containing *A mathematical theory of random migration* [3]. Lotka (1924) [4] and Volterra (1926) [5] proposed independently nonlinear interactions between different species and obtained non-trigonometric periodic solutions. As the relation between populations of predators and prey it represents one of the first models in mathematical ecology. Similar considerations for relations between sane, infected and recovered people give rise to the Kermack-McKendrick model (1927) [6], an early prototype for studies of epidemic outbreaks.

In the 1950s and 60s nonlinear models like the Hodgkin-Huxley and the Fitzhugh-Nagumo model started to explain neuronal cells and they account for effects like spiking and bursting. A freely available source on neuron dynamics is *Dynamical Systems in Neuroscience* by Eugene M. Izhikevich (2007) [7].

When a (non-linear) dynamical system is subject to a weak periodic forcing it might show large-scale fluctuations entrained to the periodicity of the "signal". If the response is enhanced or induced by random fluctuations the effect is known as stochastic resonance. Although in 1981 it was initially proposed to account for the 100.000 year periodicity in the Earth's ice ages, the first experimental demonstration of stochastic resonance was with an electronic device called the Schmitt trigger in 1983. In a living system stochastic resonance was shown at first with single mechanoreceptor cells from crayfish (1993). A Review of stochastic resonance is found in Gammaitoni et al. (1998) [8]. Russell et al. (1999) [9] showed that the juvenile paddlefish, which locate their single prey with an electrosensory antenna, have enhanced capture capabilities when an optimal level of electric noise is added to their environment. Furthermore, Freund et al. (2002) [10] investigated how the sum of the swarm's uncorrelated electric fields could generate the necessary noise for enhancing the weak signal of a single animal swimming outside the swarm.

As a side effect of these paddlefish experiments at the *Center for Neurodynamics* in the *University of Missouri at St Louis* (USA) the group's attention was drawn to the swarming behaviour of paddlefish's preferred prey, the *Daphnia*. The animal's limited perception of the whole population does not hinder a coherent movement under certain circumstances. Swarming is known from many animals and much theoretical and experimental activity to reveal the basic mechanisms has been pursued.

When the knowledge of stochastic and nonlinear dynamical systems is applied to chemical reactions, a lot of cellular and subcellular processes can be studied. For example Thattai et al. showed how negative feedback in gene transcription can efficiently decrease system noise (2001) [11]. Enzyme kinetics, another dynamical system, have a long history. The experimental work of Lu et al. (1998) [12] prove the existence of fluctuations inherent in the enzymatic turnover rate of cholesterol oxidase, as well along many turnovers of a single enzyme as in comparison with other (structurally identical) enzyme molecules.

As a consequence of growing interdisciplinarity in modern science many projects require the cooperation of scientists with different backgrounds. In December 2004 the European Commission initiated *BioSim*, a *Network of Excellence*. It joins the forces of pharmacokinetics, computer simulation and complex systems theory in a network to "...develop *in silico* simulation models of cellular, physiological and pharmacological processes to provide a deeper understanding of the biological processes..."¹. The many academic partners study a variety of problems: the "deep brain stimulation" is a technique used to tackle several neurological diseases which focuses on the desynchronization of neuronal cells, "Modelling of molecular regulatory mechanisms of circadian rhythms" looks for the underlying mechanisms that control biological rhythms, "Models of mental diseases and sleep regulation" aims to shed light on the regulatory networks of hormones and other factors in mental disorders. This is to name just a few of the fields of investigation in *BioSim*.

The development of therapies undergoes a long and difficult way. When a chemical compound is found to be a candidate for some cure, one of the many steps in development has to determine the bioavailability of the drug: the fraction of administered dose of unchanged drug that reaches the circulation. This is partly determined by the ability of the drug to pass into the body (through the skin, intestine, lung etc.). Much experimental activity is carried out to study these mechanisms.

The presented work was supported financially by the *BioSim* network of excellence and the Government of the Balearic Islands. Scientific, logistic and moral assistance came from the IFISC.

¹<http://www.biosim-network.net/>

Chapter 1

Introduction

This work deals with two different fields of research. The first is dedicated to the modelling of motion found in biology. We will give a short introduction to the topic and present two possible ways to describe biological motion. Both were inspired by the research on swarming in the *Humboldt University Berlin* and applied to model the motion of the water flea (*Daphnia*). One of them is presented in more detail in chapter 2. The second field of research is related to the work at the IFISC (UIB-CSIC) within the BioSim network. It is about drug absorption through cell monolayers. In this introduction we will introduce some aspects of biological research at the level of dynamical systems and present the results from the analysis of a drug absorption model in chapter 3.

1.1 Motion in biology as a dynamical system

In the preface we mentioned the Brownian motion which is a consequence of an external energy source known as “heat”. Brownian particles do not have internal energy, thus moving around passively. It is in contrast to real biological motion where the “particles” have an internal source of energy. Moreover, their motion does not depend only on external conditions, such as temperature, pressure etc., but on some internal conditions. For example, different goals like feeding, protection and reproduction result in different behaviours like grazing, swarming and searching. In general, biological locomotion can be seen as a continuous process (e.g. swimming fish) or discrete (hopping fleas). It can happen in a three dimensional space like the air or in two dimensions like the earth’s surface. One interesting aspect of animal motion which is worth studying is the propelling mechanism. It can be as different as the flagellar motor in some bacteria, the walk with two, four or more legs and the creeping of worms, snakes and slime molds. Another aspect concerns the way the motion is controlled internally and externally or addresses the question whether the locomotion is performed in some “optimal” way [13].

When it comes to modelling, different dynamical systems are available. If the path of motion is piecewise straight a random walker might do the job.

Below (section 1.1.1) we will introduce the basic concept of a simple random walker. Many extensions have been developed since its introduction more than a hundred years ago and nowadays the random walker can be applied to many cases, for example when the path is not really straight. These kind of models are easy to implement computationally with rapid algorithms, which is an advantage over continuous models.

In many situations, however, it is not possible to track down individual motion and one rather focuses on population densities. In this case one can take the so-called diffusion-limit and assume that the population density changes according to some diffusion-drift equation. Further down, in chapter 2, we present an example, where a diffusing population is grazing on a density of some food. Many more examples and a thorough analysis of problems and methods can be found in *Diffusion and Ecological Problems: Modern Perspectives* by Akira Okubo [14].

A third way, and from the physicist point of view probably the most convenient one, is the description by means of Newtonian equations of motion - differential equations describing the motion of individual particles (animals, plants, bacteria etc.). If these equations are deterministic the initial conditions determine the whole trajectory. Since the biological environment is usually not deterministic, stochastic differential equations are a better approach. They go back to the work of Paul Langevin. A special model of stochastic differential equation, which was used successfully to explain the display of swarming motion, is introduced in section 1.1.2.

Another class of models which allow the description of some biological motion is the class of cellular automata. They are described as systems in a spacial grid where the locations are occupied by state variables. The variables change their values at discrete time steps according to some deterministic or stochastic rule. Although it is not described in detail here we want to mention it, at first because it is similar to the random walker model and second because it allowed for the first time the description of gliding and aggregation effects of myxobacteria [15].

It follows the introduction of the random walker and that of the active Brownian particles.

1.1.1 Random walkers

The random walker model goes back to the work of Karl Pearson in the year 1905 [16]. He asked for the probability to find a drunk man the morning after he left the bar, when had been doing steps of constant length in arbitrary direction throughout the night. Rayleigh answered that he had found the solution in a different context about 15 years earlier and the highest probability to find the man is in front of the bar were he started his walk home.

Let's have a look at the basic ingredients. A random walker as proposed by Pearson is a (point like) agent which moves at discrete moments i a certain

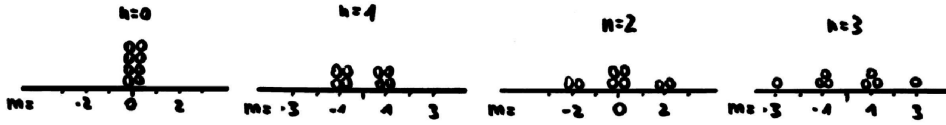


Figure 1.1: Four steps of eight random walkers. This is the most probable realisation. One sees that most particles are found at the origin.

vector \vec{r}_i . This vector has constant length but the direction is chosen at random. In one dimension this obtains a very simple structure since this motion leads to a discrete space as well (fig. 1.1).

Written in mathematical terms, the displacement vector of this simple model in one dimension is

$$r_i = \begin{cases} +1 & \text{with } p = \frac{1}{2} \\ -1 & \text{with } p = \frac{1}{2} \end{cases}. \quad (1.1)$$

The probability for each possible direction is called p . If this uncorrelated walker starts at $r_{t=0} = 0$ then the position of the walker after an even (odd) number of steps is even (odd, respectively). Therefore both, the sum and the difference of step number n and position m , will be an even number always. If we call the number of steps to the left l and the number of steps to the right r , we obtain:

$$n = r + l, \quad m = r - l, \quad (1.2)$$

OR

$$r = (n + m)/2, \quad l = (n - m)/2. \quad (1.3)$$

l and r are well defined by n and m but for every (n, m) there is a number of possible paths, i.e. of possible sequences of steps to the right and to the left. The number of possible paths $P(n, m)$ is

$$P(n, m) = \frac{n!}{r!l!} \quad (1.4)$$

and from (1.3) follows

$$P(n, m) = \frac{n!}{\left(\frac{n+m}{2}\right)! \left(\frac{n-m}{2}\right)!}. \quad (1.5)$$

This equation has to be normalised by the number of all possible paths with n steps (2^n) to find the probability $p(n, m)$ for a walker to be at position m after n steps:

$$p(n, m) = \frac{1}{2^n} \frac{n!}{\left(\frac{n+m}{2}\right)! \left(\frac{n-m}{2}\right)!}. \quad (1.6)$$

This binomial distribution has a limit for large n which is found with the Stirling's approximation to be

$$p(n, m) \approx \frac{1}{\sqrt{2n\pi}} e^{-\frac{m^2}{2n}}. \quad (1.7)$$

Now we will use this expression for long time to quantify the dynamics. The mean squared distance is calculated to:

$$\langle m^2 \rangle = \int_{-\infty}^{\infty} m^2 \frac{1}{\sqrt{2n\pi}} e^{-\frac{m^2}{2n}} dm = n. \quad (1.8)$$

It is proportional to time (step n), a result which coincides with Fick's diffusion. Therefore a walker starting at the origin will be with a probability of 68% within the interval $[-\sqrt{n}, \sqrt{n}]$ after n steps.

1.1.2 Active Brownian particles

The base of active Brownian particles is the Langevin-equation which in turn goes back to a Newtonian equation of motion ($\vec{F} = m\vec{a}$) with an additional force of fluctuating character. In its simplest form the force is made up of linear (Stokes') friction kv plus the fluctuating term $\xi(t)$:

$$m\dot{v} = -kv + \xi(t). \quad (1.9)$$

v is the velocity, i.e. the temporal derivative of position x . The nature of ξ is subject to a lot of investigation and here we cannot go into too many details. When ξ is a force as a consequence of uncorrelated collisions (as for the concept of Brownian motion) one considers that accelerating and slowing parts are equally distributed. In other words, the mean over time is zero:

$$\langle \xi(t) \rangle_t = 0. \quad (1.10)$$

In addition it is supposed to be δ -correlated, so that we can write

$$\langle \xi(t)\xi(t+\tau) \rangle_t = 2D\delta(\tau). \quad (1.11)$$

Under these conditions the mean squared distance of many realisations for eq. (1.9) can be solved to:

$$\langle x^2 \rangle = \frac{2D}{km}t, \quad (1.12)$$

the linear connection known from free, or passive, diffusion processes. It is the solution of the Brownian particle.

In the general case the friction does not have to be constant. One could write:

$$\dot{v} = f(v) + \xi(t) \quad (1.13)$$

or, if $f(v)$ can be written as the derivative of a potential $U(v)$, as

$$\dot{v} = -\frac{\partial U}{\partial v} + \xi(t). \quad (1.14)$$

If $f(v)$ is a (piecewise) integrable function, one finds as stationary probability distribution for v :

$$P_{st}(v) = Ne^{\frac{1}{D} \int f(v) dv} = Ne^{-\frac{U(v)}{D}}. \quad (1.15)$$

If we consider the particle to have an internal energy source, thus moving on its own behalf and only additionally being disturbed by a random force, we obtain the *active Brownian particle* [17]. Instead of a linear friction as in (1.9) one puts a nonlinear friction

$$k(v) = -\alpha + v^2, \quad (1.16)$$

which describes a source of energy for a velocity lower than α and a dissipation otherwise. The absolute value of the stationary velocity is $\sqrt{\alpha}$.

Additional forces can be added to the Newtonian equations (1.9) and (1.13). In this way one can add correlation to the direction of motion or terms like the flow of surrounding media.

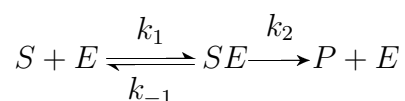
1.2 Biochemical and biophysical reactions

Biochemical and biophysical processes are probably the lowest level of description of living systems. Ion channels, synaptic connections, the propagation of information in form of electric currents in neuronal cells, photosynthesis, enzymatic reactions, absorption and dissolution, transcription and translation of DNA and many more; all are elementary processes in biology, described by chemical reactions and physical processes. Some of these processes are topic of this work.

At the turn of the eighteenth century the meat digestion by stomach secretions or the conversion of starch to sugar by saliva were known effects. However, the underlying mechanism had not been identified. Identification of “nonliving” substances produced by living organisms took until the end of that century when the term “enzyme” was coined. It is still a large field of interest now and the kinetics of enzymatic reactions are similar to some processes in drug absorption. For that reason we will now introduce the dynamical system for basic enzyme reactions and will introduce a system with identical dynamics in the section on drug absorption models.

1.2.1 Simple enzyme reactions

Enzymes are molecules that regulate reaction rates by changing the activation energy for a given chemical process. In the simplest form this can be described with the following reaction equation:



The idea is that a substrate molecule S binds to an enzyme molecule E and together they form the complex SE . k_1 and k_{-1} determine the rate of the reaction. The complex decays with rate k_2 into the product molecule P and

the enzyme. In fact in some cases the complex decays into P and a refractory conformation of E which then goes back into the ground state. If this is a fast process it can be neglected. The product P is typically quickly absorbed into the background, therefore the rate k_{-2} can be neglected as well. The reaction equation can be written as a dynamical system. Using lowercase letters for concentrations ($c(t)$ for the complex concentration) we find:

$$\dot{s}(t) = k_1c(t) - k_1s(t)e(t) \quad (1.17)$$

$$\dot{e}(t) = (k_{-1} + k_2)c(t) - k_1s(t)e(t) \quad (1.18)$$

$$\dot{c}(t) = -(k_{-1} + k_2)c(t) + k_1s(t)e(t) \quad (1.19)$$

$$\dot{p}(t) = k_2c(t) \quad (1.20)$$

If there are a lot of substrate molecules present one can assume its concentration to be rather constant, i.e. $\dot{s}(t) \approx 0$. After some transient time the process will reach some steady production flow and the same amount of complex is generated as it decays. This means the concentration $c(t)$ is constant ($\dot{c}(t) \approx 0$) and we can eliminate another variable. We obtain from (1.19):

$$c(t) = \frac{k_1s(t)e(t)}{k_{-1} + k_2}. \quad (1.21)$$

With no complex molecule initially present ($c_{t=0} = 0$) we know that the sum of complex plus enzyme will be constant ($c(t) + e(t) = e_0$). Replacing $e(t)$ in above equation the time course of c is

$$c(t) = \frac{e_0s(t)}{s(t) + \frac{k_{-1} + k_2}{k_1}} \equiv \frac{e_0s(t)}{s(t) + K_m} \quad (1.22)$$

and when put into (1.20) one gets the product generation:

$$\dot{p}(t) = \frac{k_2e_0s(t)}{s(t) + K_m} \equiv V_{max} \frac{s(t)}{s(t) + K_m}. \quad (1.23)$$

V_{max} is the maximum production rate and K_M is called the Michaelis constant. It denotes the concentration where the production rate reaches half of its maximum value. Equation (1.23) was first derived by Michaelis and Menten in 1913 [18]. Although it is presented here in the context of enzymatic reactions, we will see further down that it is used to describe other bind-react-release types of processes.

1.3 Drug absorption

Orally administered drugs are mainly absorbed in the small intestine. The molecules have to pass through the epithelial cells where, depending on drug composition and size, a variety of processes act upon the molecules [19]:

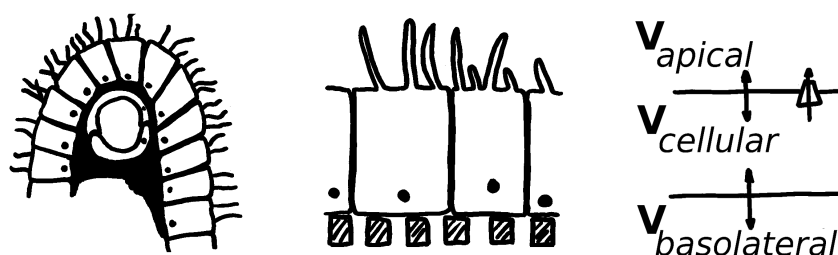


Figure 1.2: From the small intestine to the three-compartment model. *left:* small intestine with lamina propria and embedded capillary, *middle:* Schematic view of mono layer experiment. *right:* Sketch of mathematical model.

Due to the *tight junctions* which connect epithelial cells among each other, only very small and hydrophilic molecules can pass along the contact of two cells (*paracellular* route). Therefore transport along this pathway is very small except for when a modulator of tight junctions is present. If the compound has the appropriate physical and chemical properties it can cross the cell's membranes passively (*transcellular passive diffusion*). These compounds may be substrate for intracellular metabolism and they are more likely to be substrate for efflux transporters, extracting them from the cell back into the intestine. However, the transcellular passive way (limited by efflux transporters) is the main route of absorption for orally taken drugs. In other cases transcellular absorption can be mediated by naturally occurring carriers which normally transport vitamins or nutrients. A rather seldom pathway in adult small intestine absorption is via *endocytosis*, where the transported material is coated with part of the cell membrane on one side, incorporated into the cell and then released from the cell on the other side.

When it is inside the small intestine the drug has to be considered outside the body. On the other side of the epithelial cells the drug is inside the body. It reaches the *lamina propria* and passes from there into the blood stream in the capillaries (fig. 1.2 (left)).

Much experimental activity aimed at analysing the kinetic aspects of the process of drug absorption has been pursued recently. For better control, a variety of *in-vitro* methods on drug absorption have been developed [20]. Epithelial cell cultures can be seeded in a mono-layer on semipermeable membranes, forming the contact surface of two little pots (fig. 1.2 (middle)). Concentrations of an applied drug can be measured over time in both chambers.

Two well known cell culture models are Caco-2 cells [21] and MDCK cells [22]. Caco-2 cells were derived from a human colon carcinoma. After they are seeded they differentiate into an "...highly functionalized epithelial barrier with remarkable morphological and biochemical similarity to small intestine columnal epithelium." [22]. Therefore they are used to assess transport properties of new developed compounds. The MDCK cell line was derived from canine kidney cells and as well differentiates into epithelium and form

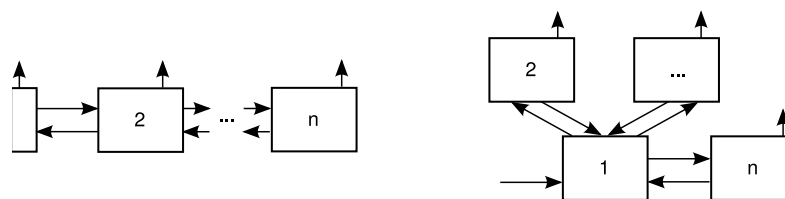


Figure 1.3: Comparison between catenary (*left*) and mammillary (*right*) compartment models.

tight junctions. One downside of these cell models is that they are seeded on a flat surface, whereas the intestine forms folded walls with much higher surface area than just the inside of a tube. As a consequence only high permeability drugs are well represented by this model, whereas the permeability for low permeability drugs is underestimated when compared with *in vivo* values [23].

A layer seeded in this way is a monocellular layer, in direct contact with the liquids above and below through the semipermeable membrane. It suggests modelling with a set of compartments.

1.3.1 Compartment models

Trying to break systems of drug action down into smaller units, pharmacology came up with the so-called compartment models. A number of compartments are connected with each other in different ways and the mass flux of a given substance through the system is the object of interest. The models can be split into classes according to their topology. The catenary models ('catena' *Latin* = 'chain') are compartments connected in a row whereas the mammillary models have a central compartment with others surrounding it (fig. 1.3). A mix of both types is possible as well. A different form of classification looks at the level of abstraction, i.e. that if the compartments correspond to a well defined volume in the organism the model is said to be physiological whereas other models, where no such correspondence exists, are called mechanistic models [24]. The considerations in chapter 3 will concern a purely catenary model and we do not distinguish between physiological and mechanistic model. The presented method applies to both classes. However, the experimental work we have chosen to compare our theory with is about a physiological one.

The data of absorption experiments, with cell cultures mentioned in above section, is usually compared with compartment models where some specific simplifications are in order: It is considered that two volumes (e.g. gastrointestinal lumen and blood plasma *in-vivo* or apical and basolateral chamber *in-vitro*) are connected through a third, *in-vitro*: cellular, volume. One contact has additional flux depending non-linearly on one concentration. When applying to *in-vitro* experiments, it is assumed that the concentrations in the different cells of the mono-layer are equal (which is exact only if all cells have

the same parameters), such that the absorption can be seen as a transport from one large volume to another through a third (the cellular) volume [25]. Figure 1.2 (right) sketches the simplifications of the model. There is no spatial dependence and molecules can pass through the two cell membranes. The overall amount of drug molecules is considered to be constant, a hypothesis that assumes a closed system and that metabolism does not occur. In practise, those conditions are fulfilled if the experiment does not last for a very long time. The result is a three-compartment model; a model that describes the behaviour of solutions or emulsions in connected volumes by analysing the molecule flux in between them and all sources and sinks.

1.3.2 Multi Drug Resistance (MDR) transporter

Absorption of many drugs is seriously limited by P-glycoprotein (P-gp), the multidrug transporter [26]. It acts upon a broad spectrum of chemical compounds and limits their absorption drastically. Especially in cancer cells an overexpression of this protein leads to resistance to the drug.

This particular protein (fig. 1.4) is expressed on the apical membrane of intestinal epithelium cells [27, 28, 29]. The molecule to be transported has to bind on the protein and will then be “flipped” [19] onto the other side of the membrane, where it is no more available for the “reaction”. This makes its dynamics similar to enzyme reactions and therefore the flow \mathcal{J} of chemicals is often represented by the sigmoid shape of a Michaelis-Menten reaction-rate (1.23):

$$\mathcal{J}(Q_C) = \frac{SV_M Q_C/V_C}{K_M + Q_C/V_C}. \quad (1.24)$$

V_M determines the maximal reaction velocity, S is the surface area and K_M is the concentration for which the velocity reaches half of the maximum. In this **intracellular binding**, the relevant variable is the concentration Q_C/V_C around the binding site of the transporter, inside the cell.

In other cases, the efflux pump has an **extracellular binding** site. Consequently, the transport is determined by the drug concentration, Q_A/V_A , in

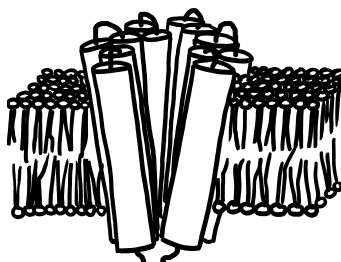


Figure 1.4: Schematic view of the P-gp transporter protein. It penetrates inner and outer leaflet of the cellular membrane.

the apical compartment and corresponding Michaelis-Menten expression is:

$$\mathcal{J}(Q_A) = \frac{SV_M Q_A / V_A}{K_M + Q_A / V_A}. \quad (1.25)$$

Both, eq. (1.24) and (1.25) are known from section 1.2.1 and will be discussed in detail in chapter 3.

1.4 Outline

In the preceding sections of the introduction we have presented a small selection of known dynamical systems which were constructed to describe effects observed in the living nature.

The random walker (sec. 1.1.1) can be extended in many ways. A special way, with correlated step directions, was developed in chapter 2. It was used for describing the movement of water fleas. The concept of active Brownian particles will not be detailed any further than was presented in sec. 1.1.2, however, it was shown that when modelled in this way, a population can be described as a continuous concentration diffusing in space. This idea has been put into relation with food uptake of animals, grazing in large populations (sec. 2.2).

We have seen how drug absorption experiments can be described by modelling the flux between three compartments (sec. 1.3). The respective dynamical system will be constructed in chapter 3, where a transformation into a problem from classical mechanics is applied and an adequate approximation proposed. We will give analytical expressions for the concentration development in the different compartments.

Chapter 2

The Daphnia

The *Daphnia* is a 2-4 mm large crustacean like crabs, lobsters and crayfish are (fig. 2.1, left) and is prey to a variety of larger animals. It moves with a velocity of 4 to 16 mm/s through the water and maintains a rather constant depth. Under certain light conditions and the presence of *kairomones* (chemical substances originating from the predator) *Daphnia* start moving in a coherent fashion, swirling around a common vertical centre in a common circling direction [30, 31, 32]. Minimal requirements for for swarming to occur were investigated by e.g. [33, 34, 35].

When *Daphnia* are studied individually, without light and without kairomones, obviously they display a different motion. About intention one can only speculate, however, the movement is not uncorrelated. They direct their swim strokes slightly upwards to balance negative buoyancy and change horizontal direction in a way which prefers angles between successive strokes of around 30° (see fig. 2.1, right). Other crustacean have shown a similar distribution [37]. When one models the movement as a sequence of constant steps in a plane, with one-step correlated turning angles, one can show that the mean square distance approaches a linear asymptote. The proportionality

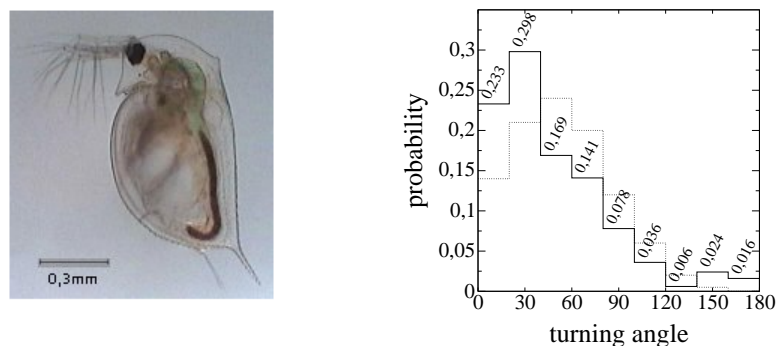


Figure 2.1: left: Picture of a *Daphnia* from [36]. right: distribution of angles between successive hops (black line) and comparison with a Gaussian distribution of same mean and variance (mean 48° , variance 36°). Data from [30], 1600 moves from tracks of eight different *Daphnia*

can be calculated straight from the distribution and one can determine the time it takes to approach the line. This was carried out in [38] and in the following section we want to give a short summary of the results.

In the last section of this chapter we summarised a very simple model for a diffusing species grazing on a not growing and not moving food supply. Depending on initial food distribution and grazing rate the consumed food shows a maximum for a certain spacial diffusion coefficient. These results are part of [39], where results from [38] could be reproduced qualitatively using the concept of *active Brownian particles* [17], rather than that of random walkers.

2.1 Daphnia as random walkers

The hopping movement of the animal suggests a discrete description of the process. The standard random walker was described in an earlier section. In order to model the correlated direction changes as observed in the experiment, we propose the following random walker

$$\vec{r}_i = \begin{pmatrix} \lambda \cos \theta_i \\ \lambda \sin \theta_i \end{pmatrix} \quad (2.1)$$

$$\theta_i = \theta_{i-1} + \eta_i, \quad (2.2)$$

where λ is the constant step length and η_i is a random number drawn from a distribution $f(\eta)$.

After n steps the mean squared displacement is the sum of all steps and when averaged over a large ensemble one finds

$$\begin{aligned} \langle \vec{R}_n^2 \rangle &= \left\langle \left(\sum_{i=1}^n \vec{r}_i \right)^2 \right\rangle \\ &= n\lambda^2 + 2\lambda^2 \sum_{i=1}^{n-1} \sum_{j>1}^n \langle \cos(\theta_i - \theta_j) \rangle. \end{aligned} \quad (2.3)$$

Defining the angular correlation γ as

$$\gamma = \langle \cos(\theta_i - \theta_{i+1}) \rangle = \langle \cos \eta \rangle = \int_{-\pi}^{\pi} f(\eta) \cos \eta d\eta \quad (2.4)$$

and excluding correlation over more than one step one can show that

$$\langle \cos(\theta_i - \theta_{i+s}) \rangle = \gamma^s. \quad (2.5)$$

With this equation (2.3) reduces to:

$$\langle \vec{R}_n^2 \rangle = \lambda^2 \left(n \frac{1+\gamma}{1-\gamma} - 2\gamma \frac{1-\gamma^n}{(1-\gamma)^2} \right), \quad (2.6)$$

a relationship which was derived first by Kareiva and Shigesada [40]. We see that the averaged motion depends only on the angular correlation γ . Since $|\gamma| < 1$ the second term on the right hand side will be a constant for large n . Simulation of random walker populations and the solution of (2.6) are compared in fig. 2.2, left. The linear regime and how it is approached is shown as well. When the dependence is linear one can give a diffusion coefficient D as

$$4D = \frac{1 + \gamma}{1 - \gamma} \frac{\lambda^2}{\tau}, \quad (2.7)$$

with τ defined as the duration of each step. We call

$$D_n = \frac{1 + \gamma}{1 - \gamma} \quad (2.8)$$

the *reduced diffusion coefficient* which is greater than one if the diffusion is faster than for the uncorrelated case and between 0 and 1 for slower diffusion.

How many steps does it take until the time dependence in the second term of (2.6) vanishes? If we think of a line parallel to the asymptote we can ask for when the averaged trajectory will cross this line. Setting the distance of the two lines to a fraction ϵ of

$$e = \frac{2\gamma}{(1 - \gamma)^2} \quad (2.9)$$

we require:

$$D_n n - e + e\gamma^n \doteq D_n n - e + \epsilon e \quad (2.10)$$

and find

$$n_{\text{crossover}} = \frac{\ln \epsilon}{\ln \gamma}. \quad (2.11)$$

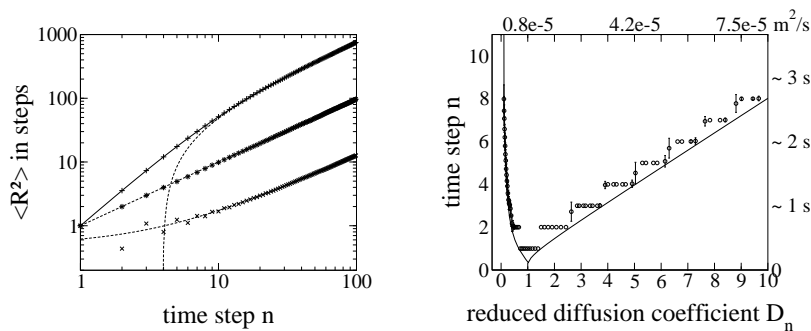


Figure 2.2: left: simulation of 1000 random walkers with Gaussian angular distribution (mean: 10° (+), 90° (*), 170° (x); variance 36° for all. Line is analytic solution according to (2.6), dashed line is linear asymptote. right: Time needed to approach the asymptote. Line according to (2.11). 500 simulations of 5000 random walkers, $\epsilon = 0.2$. The axes have alternative dimensions for real *Daphnia* parameter ($\tau = \frac{1}{3}$ s, $\lambda = \frac{10}{3}$ mm). D_n for the experimental angle distribution is 3.1.

This relationship is compared with simulations in fig. 2.2, right. The step like behaviour of the simulation data is owed to the discrete nature of a random walker, apart from that one finds good coincidence.

As we have seen before, the obtained results depend on the angular correlation γ so we will explicitly calculate this value for two different types of distributions.

2.1.1 Two angles

In the histogram of turning angles (figure 2.1) we can see that backward jumps are exercised and, moreover, that another local maximum of probability for backward jumps exists. Maximal probability is centred around 150° and it accounts for roughly a tenth of the occurrences of the main peak. Thus we propose a angular distribution $f(\eta)$ composed of two δ -peaks

$$f(\eta) = \frac{1}{2} [a \delta(|\eta| - \eta_1) + (1 - a) \delta(|\eta| - \eta_2)] \quad (2.12)$$

with a controlling the relative weight and η_1 and η_2 positions of the peaks. γ is easily derived to

$$\gamma = a \cos \eta_1 + (1 - a) \cos \eta_2. \quad (2.13)$$

The reduced diffusion coefficient as a function of γ for this solution is shown in the left graph of figure 2.3. With the larger peak fixed to the maximum in the experimental distribution (48°) the position of the second peak is crucial to the diffusion coefficient. Increasing $\eta_2 > \eta_1$ the enhanced diffusion is damped up to 40%.

2.1.2 Gaussian distribution

If the turning angles are distributed according to a Gaussian function with mean $\langle \eta \rangle$ and variance σ the angular correlation γ can be determined as well.

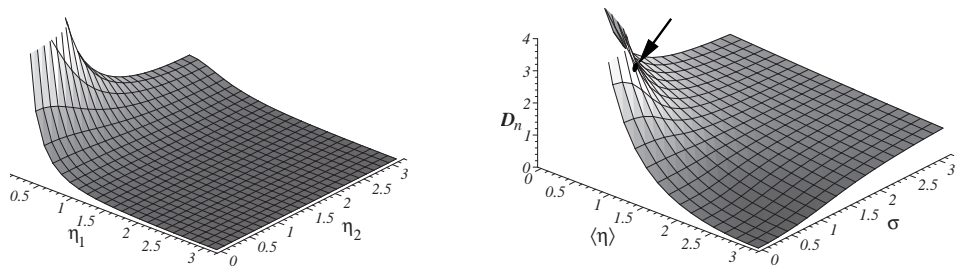


Figure 2.3: Reduced diffusion coefficient for two δ -peaks with a weight of 10:1 *left* and for Gaussian distributed turning angles *right*. The arrow marks D_n for the values obtained in the experiment.

Carrying out the integration in (2.4) one comes up with the term

$$\gamma(\langle\eta\rangle, \sigma) = \frac{\cos\langle\eta\rangle \cdot \Re[\operatorname{erf}(b) - \operatorname{erf}(c)] - \sin\langle\eta\rangle \cdot \Im[\operatorname{erf}(b) - \operatorname{erf}(c)]}{e^{\frac{\sigma^2}{2}} \left[\operatorname{erf}\left(\frac{\pi - \langle\eta\rangle}{\sqrt{2}\sigma}\right) + \operatorname{erf}\left(\frac{\langle\eta\rangle}{\sqrt{2}\sigma}\right) \right]} \quad (2.14)$$

The terms $b = \frac{\langle\eta\rangle + i\sigma^2}{\sqrt{2}\sigma}$ and $c = \frac{-\pi + \langle\eta\rangle + i\sigma^2}{\sqrt{2}\sigma}$ are replaced to give a more concise formula. \Re and \Im denote the real and imaginary part, consequences of the obtained complex error function, and we have a real function for all $\langle\eta\rangle$ and σ . Introducing (2.14) into (2.8) one obtains the reduced diffusion coefficient (see right graph in fig. 2.3). In the case of $\langle\eta\rangle = \pi/2$ we have $\gamma = 0$ and therefore $D_n = 1$. This is equal to the value of free diffusion and does not depend on the variance. The reduced diffusion coefficient of the *Daphnia* is 3.1, indicating a diffusion three times faster than a free diffusing particle.

2.2 A food model

Here we want to develop a simple approach on how much food a single animal could consume along its path. Although not limited to *Daphnia* it was created in that context and therefore we will present it here.

The model assumes an animal density $\rho(\vec{r}, t)$ which obeys a diffusion equation of constant spacial diffusion coefficient D

$$\frac{\partial\rho}{\partial t} = D\Delta\rho. \quad (2.15)$$

A random walker as presented above seems a crude realisation for (2.15) but if the step size is small enough in relation to the system size it should be an appropriate assumption. Furthermore, in [39] a way is shown which maps the *Daphnia* motion with its angular correlation to the continuous model of an active Brownian particle. As such the density ρ and a continuous expression for the diffusion is exact. The solution of the resulting density in two dimensions is

$$\rho(\vec{r}, t) = \frac{1}{4\pi Dt} \exp\left[-\frac{r^2}{4Dt}\right]. \quad (2.16)$$

If we consider now that along their path the particles of density ρ consume food C of density $c(\vec{r}, t)$ at constant rate k , then the food density is described by the dynamics

$$\frac{\partial}{\partial t}c(\vec{r}, t) = -kc(\vec{r}, t)\rho(\vec{r}, t). \quad (2.17)$$

When ρ is replaced by eq. (2.16) the latter equation can be solved exactly. In terms of the exponential integral [41], $E_1(a) = \int_a^\infty \frac{e^{-t}}{t} dt$, the solution is given as

$$c(\vec{r}, t) = c_0 \exp\left[-\frac{\rho}{4\pi D} E_1\left(\frac{r^2}{4Dt}\right)\right]. \quad (2.18)$$

How the food density evolves can be seen in fig. 2.4, left.

For simplicity we'll have a look at the evolution of a spherical food patch of radius R . We imagine a circle centred at the origin where the grazing species starts at $t = 0$ with its highest density. Outside the circle no food is found. The food which is left over after a time T is obtained by integrating (2.18) over space and time:

$$C(T, R, D) = 2\pi c_0 \int_0^R \exp \left[-\frac{k}{4\pi D} E_1 \left(\frac{r^2}{4DT} \right) \right] r dr. \quad (2.19)$$

The right graph in figure 2.4 shows this result for different grazing rates and a minimum in the curve determines a diffusion constant where most food is ingested. Since the diffusion coefficient in the random walker model presented above depends monotonously on the mean turning angle it implies a minimum with respect to the turning angle as well. If the mean turning angle is too small, animals move in a rather straight line and leave the food patch too fast. On the other hand if the turning angle is too large, the hopping stays a too long time on the same spot and consumes all present food. Therefore an optimum is observed.

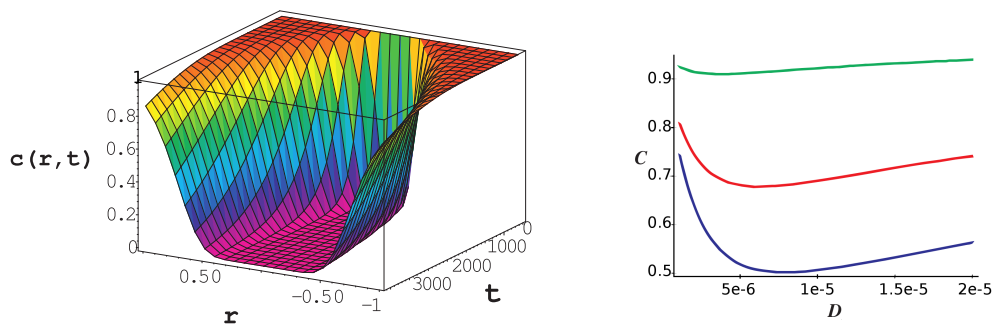


Figure 2.4: left: evolution of food density along a straight line for diffusing species released at $r = 0$. right: left over food after fixed time T within a path of fixed radio. Different lines for different feeding pace k . The curve clearly shows a minimum.

Chapter 3

A Three-Compartment Model

In the introduction it was reported that drug absorption experiments are often modelled by a three-compartment model. Now we will see, how the according dynamical system is constructed. Then it can be transformed into a problem in classical mechanics, suggesting an appropriate approximation: a damped linear oscillator.

Further down this method is applied to a specific form of non-linearity, used to represent the efflux of the multi drug resistance transporter P-gp. The results are compared with an absorption experiment done with an antibiotic. The solution allows to analyse the influence of the physiological parameters on the measurements and the propagation of errors and diversity in the parameters through the process.

In the last section of the present chapter we have a quick look on a three-compartment model with an additional parameter which stands for the retention of drug molecules within the cell.

3.1 Model and method

Passive transport across the membrane is mediated, to a first approximation, by the concentration gradients according to FICK's law [42], which specifies a linear relation between the flux of particles and the concentration gradient. When the passive absorption is accompanied by energy consuming efflux transporters, it is represented by a non-linear function term in the kinetic transport equations. A variety of transporter types could be involved in the absorption of the molecules. In our work we consider that the non-linear transporters are present only on one (the apical) cell membrane, but our results could be extended straightforwardly to the case that those transporters are located on the basolateral membrane (or even in both membranes). Including both linear and non-linear terms, the time evolution of the amount of diluted molecules ($Q_{A/C/B}$) in the three compartments can be described as

follows:

$$\frac{dQ_A(t)}{dt} = +Cl_{AC} \left(\frac{Q_C}{V_C} - \frac{Q_A}{V_A} \right) + \mathcal{J} \quad (3.1)$$

$$\frac{dQ_C(t)}{dt} = -Cl_{AC} \left(\frac{Q_C}{V_C} - \frac{Q_A}{V_A} \right) - \mathcal{J} - Cl_{CB} \left(\frac{Q_C}{V_C} - \frac{Q_B}{V_B} \right) \quad (3.2)$$

$$\frac{dQ_B(t)}{dt} = +Cl_{CB} \left(\frac{Q_C}{V_C} - \frac{Q_B}{V_B} \right) \quad (3.3)$$

$$Q_0 = Q_A + Q_B + Q_C, \quad (3.4)$$

where equation (3.4) stands for the conservation of overall molecule number, Q_0 . The indices denote the corresponding compartment (**A**pical, **C**ellular, **B**asolateral), $V_{A/C/B}$ are the respective volumes. The apical, cellular and basolateral concentrations are given respectively by $a = Q_A/V_A$, $c = Q_C/V_C$ and $b = Q_B/V_B$. The passive, linear, diffusion terms are proportional to the concentration difference, being Cl_{AC} and Cl_{CB} the clearances indexed with their respective membrane index. In the equations, \mathcal{J} represents the non-linear contribution due to specific efflux transporters, depending either on Q_A or Q_C . As it is an energy-consuming process, this can happen both along or against the gradient.

3.1.1 Potential and friction

Due to the supposed conservation of mass the system (3.1-3.4) has only two degrees of freedom. In other words: it can always be represented by two differential equations of first order or by one differential equation of second order. With rescaled concentrations and a rescaled time s the set of equations is:

$$\dot{x}(s) = \frac{dx(s)}{ds} = a_{11}x + a_{12}y + a_{13} + j(x) \quad (3.5)$$

$$\dot{y}(s) = \frac{dy(s)}{ds} = a_{21}x + a_{22}y + a_{23}. \quad (3.6)$$

The exact appearance of the factors a_{ij} is determined by the dependent variable of the original function \mathcal{J} . If it is Q_C (*intracellular* binding sites) the variable x is the (rescaled) concentration inside the cell, if it is Q_A (*extracellular* binding site) the variable x is the (rescaled) concentration in the apical compartment (see section 3.2.1). The rescaling factor has to be chosen for a specific non-linear function \mathcal{J} and will be shown later. The factors are summarised in table 3.1.

Now, if we differentiate (3.5) with respect to s and replace in the resulting expression $\dot{x}(s)$ with (3.5) and $\dot{y}(s)$ with (3.6) we obtain a differential equation of second order. Collecting the terms one can write:

Table 3.1: Coefficients for equations (3.5-3.6). V_I is the volume of compartment where the drug is loaded initially and c_0 is the rescaled initial condition.

Parameter	INTRACellular	EXTRACellular
a_{11}	$-\left[\frac{V_B}{V_C} + \frac{Cl_{AC}}{Cl_{CB}} \left(\frac{V_B}{V_C} + \frac{V_B}{V_A}\right)\right]$	$-\frac{Cl_{AC}}{Cl_{CB}} \left(\frac{V_B}{V_C} + \frac{V_B}{V_A}\right)$
a_{12}	$\frac{V_B}{V_C} \left(1 - \frac{Cl_{AC}}{Cl_{CB}} \frac{V_B}{V_A}\right)$	$-\frac{Cl_{AC}}{Cl_{CB}} \frac{V_B^2}{V_A V_C}$
a_{13}	$\frac{Cl_{AC}}{Cl_{CB}} \frac{V_B V_I}{V_A V_C} c_0$	$\frac{Cl_{AC}}{Cl_{CB}} \frac{V_B V_I}{V_A V_C} c_0$
a_{21}	1	$-\frac{V_A}{V_C}$
a_{22}	-1	$-\left(\frac{V_B}{V_C} + 1\right)$
a_{23}	0	$c_0 \frac{V_I}{V_C}$

Table 3.2: Positive-defined, dimensionless constants determining friction and force/potential in (3.7).

Γ_0	$-a_{11} - a_{22}$	$= \frac{V_B}{V_C} + \frac{Cl_{AC}}{Cl_{CB}} \left(\frac{V_B}{V_C} + \frac{V_B}{V_A}\right) + 1$
α	$a_{12}a_{23} - a_{13}a_{22}$	$= \frac{Cl_{AC}}{Cl_{CB}} \frac{V_B V_I}{V_A V_C} c_0$
β	$a_{11}a_{22} - a_{12}a_{21}$	$= \frac{Cl_{AC}}{Cl_{CB}} \frac{V_B}{V_A V_C} (V_A + V_B + V_C)$

$$\ddot{x} = -\Gamma(x)\dot{x} + F(x), \quad (3.7)$$

with the friction coefficient $\Gamma(x)$ and the force $F(x)$ given by:

$$\Gamma(x) = \Gamma_0 - j'(x), \quad F(x) = \alpha - \beta x - a_{22}j(x). \quad (3.8)$$

Γ_0 , α and β are dimensionless and positive-defined constants, containing all information of the passive absorption process. The relation to the coefficients a_{ij} can be seen in table 3.2. Note, that only α depends on the initial concentration. The nonlinearity is only in the function $j(x)$ and its derivative $j'(x)$.

3.1.2 An approximated solution

The force in (3.7) defines a potential $V(x)$ through $F(x) = -\frac{dV(x)}{dx}$. One can try to approximate this potential by a parabola around its minimum. The quality of this approximation depends on the specific $j(x)$ but it always has the form:

$$V(x) = V_{eq} + \frac{1}{2}V''_{eq}(x - x_{eq})^2. \quad (3.9)$$

The potential's second derivative we will call ω^2 and from (3.8) we obtain:

$$V''(x_{eq}) = \omega^2 = \beta + a_{22}j'(x). \quad (3.10)$$

x_{eq} denotes the value of x at equilibrium, i.e. where the force equals zero. As a second approximation we set the friction coefficient $\Gamma(x)$ to its value in equilibrium $\Gamma_{eq} = \Gamma_0 - j'(x_{eq})$. The resulting differential equation $\ddot{x} = -\Gamma_{eq}\dot{x} - \omega^2(x - x_{eq})$ is linear and has the following solution [43]:

$$x(s) = \tilde{C}_1 e^{-s/\tau_1} + \tilde{C}_2 e^{-s/\tau_2} + x_{eq}. \quad (3.11)$$

The time scales result in:

$$\tau_1 = \frac{2}{\Gamma_{eq} - \sqrt{\Gamma_{eq}^2 - 4\omega^2}} \quad \text{and} \quad \tau_2 = \frac{2}{\Gamma_{eq} + \sqrt{\Gamma_{eq}^2 - 4\omega^2}}, \quad (3.12)$$

which will be complex whenever $\Gamma_{eq} < 2\omega$, resulting in an oscillating relaxation.

The coefficients $\tilde{C}_{1/2}$ in the solution are drawn from the initial conditions x_0 and \dot{x}_0 via eq. (3.5) replacing x and y with y_0 and x_0 . The expressions are found in table 3.3. The second variable $y(s)$ can be calculated by integrating eq. (3.6) after inserting it into the solution $x(s)$:

$$y(s) = e^{a_{22}s} \left[y_0 + \int_0^s ds' e^{-a_{22}s'} (a_{21}x(s') + a_{23}) \right], \quad (3.13)$$

which yields

$$y(s) = \tilde{D}_1 e^{-s/\tau_1} + \tilde{D}_2 e^{-s/\tau_2} + \tilde{D}_3 e^{-s/\tau_3} + y_{eq}. \quad (3.14)$$

The constants $\tilde{D}_{1/2/3}$ are found in table 3.3 as well. The third time constant is:

$$\tau_3 = -\frac{1}{a_{22}}. \quad (3.15)$$

The last dynamic variable $z(s)$ is obtained by means of the conservation law. Undoing the rescaling of concentration and time we obtain the following solution for the dissolved amount in the three compartments:

$$Q_A(t) = Q_A^{eq} - A_1 e^{-t/t_1} - A_2 e^{-t/t_2} - A_3 e^{-t/t_3} \quad (3.16)$$

$$Q_B(t) = Q_B^{eq} - B_1 e^{-t/t_1} - B_2 e^{-t/t_2} - B_3 e^{-t/t_3} \quad (3.17)$$

$$Q_C(t) = Q_C^{eq} - C_1 e^{-t/t_1} - C_2 e^{-t/t_2} - C_3 e^{-t/t_3}, \quad (3.18)$$

where the expression for the constants are collected in table 3.4.

After having solved the approximated problem, one can derive some conclusions from the solution. Although we do not know in advance how good the approximation is, we will derive some quantities. Usually pharmacological experiments do not measure the whole time course of concentrations until saturation but the so-called apparent permeability [44, 29, 45, 46, 25]:

$$P^{app} = \frac{dQ/dt}{SC_0}, \quad (3.19)$$

Table 3.3: Coefficients of dimensionless solution eqs. (3.11) and (3.14).

\tilde{C}_1	$(x_0 - x_{eq} + \tau_2 (a_{11}x_0 + a_{12}y_0 + a_{13} + j(x_0))) \frac{\tau_1}{\tau_1 - \tau_2}$
\tilde{C}_2	$x_0 - x_{eq} - \tilde{C}_1$
\tilde{D}_1	$-\frac{a_{21}\tilde{C}_1\tau_1}{a_{22}\tau_1 + 1}$
\tilde{D}_2	$-\frac{a_{21}\tilde{C}_2\tau_2}{a_{22}\tau_2 + 1}$
\tilde{D}_3	$y_0 - y_{eq} - \tilde{D}_1 - \tilde{D}_2$

where S denotes the surface area of the absorbing material. The initial concentration C_0 is loaded into one compartment and one measures the amount of material $Q(t)$ on the receiving side in the linear regime at the beginning of the process. Then the material is loaded in the opposite compartment, the amount of the substance on the receiving side is measured and then one can compare P^{app} from both directions.

The above mentioned time scales divide a process into a linear regime, an exponentially changing one and a saturation at very large times. It seems that usually one time scale t_2 can be ignored since it is very short and measurements are done after saturation of the t_2 -process [25, 44, 47]. When this is the case the apparent permeabilities are calculated to

$$P_{BA}^{app} = \frac{1}{SC_0} \left(\frac{A_1}{t_1} + \frac{A_3}{t_3} \right) \quad (3.20)$$

in the case that the drug is initially delivered in the basolateral site, and

$$P_{AB}^{app} = \frac{1}{SC_0} \left(\frac{B_1}{t_1} + \frac{B_3}{t_3} \right) \quad (3.21)$$

when the drug is delivered in the apical side. In the case that t_2 can not be omitted the expansion of (3.20) and (3.21) to the missing term is straightforward.

3.2 Michaelis-Menten type flux

In the previous section we developed a method to treat a non-linear three compartment model and proposed a way of approximating it. In this way we obtained analytic expressions for the evolution of the concentrations in the three chambers. Furthermore these solutions allow us to have specific formulas for experimentally accessible quantities, thus knowing their dependence on physiological parameters. In this section we will apply our method to a specific form of efflux used as a model flux in a variety of pharmacological

Table 3.4: Coefficients of solutions (3.16-3.18). Appearing constants \tilde{C}_i and \tilde{D}_i are shown in table 3.3. Equilibrium values in the according section of specific non-linearities. \mathcal{N} is the constant which rescales the concentration. It is chosen depending on the specific flux term.

	INTRA	EXTRA
A_1	$\mathcal{N} \left(V_C \tilde{C}_1 + V_B \tilde{D}_1 \right)$	$-\mathcal{N} V_A \tilde{C}_1$
A_2	$\mathcal{N} \left(V_C \tilde{C}_2 + V_B \tilde{D}_2 \right)$	$-\mathcal{N} V_A \tilde{C}_2$
A_3	$\mathcal{N} V_B \tilde{D}_3$	0
Q_A^{eq}	$Q_0 - \mathcal{N} (V_C x_{eq} + V_B y_{eq})$	$\mathcal{N} V_A x_{eq}$
B_1	$-\mathcal{N} V_B \tilde{D}_1$	$-\mathcal{N} V_B \tilde{D}_1$
B_2	$-\mathcal{N} V_B \tilde{D}_2$	$-\mathcal{N} V_B \tilde{D}_2$
B_3	$-\mathcal{N} V_B \tilde{D}_3$	$-\mathcal{N} V_B \tilde{D}_3$
Q_B^{eq}	$\mathcal{N} V_B y_{eq}$	$\mathcal{N} V_B y_{eq}$
C_1	$-\mathcal{N} V_C \tilde{C}_1$	$\mathcal{N} \left(V_A \tilde{C}_1 + V_B \tilde{D}_1 \right)$
C_2	$-\mathcal{N} V_C \tilde{C}_2$	$\mathcal{N} \left(V_A \tilde{C}_2 + V_B \tilde{D}_2 \right)$
C_3	0	$\mathcal{N} V_B \tilde{D}_3$
Q_C^{eq}	$\mathcal{N} V_C x_{eq}$	$Q_0 - \mathcal{N} (V_A x_{eq} + V_B y_{eq})$

absorption studies. We will use values and data from a work done recently in another group and validate the assumption of a linear regime in said experiment with our results. Furthermore we can predict for each parameter, how important it is for the measured quantities. With our method this can be done much easier than by numerically integrating the trajectories for all parameter sets, a usual practice in pharmaceutical science.

In the introduction we mentioned that drug absorption can be limited by P-gp, the multi-drug transporter. We have shown two ways of representing its dynamics, one with an intracellular binding site, another with extracellular binding site. Both situations will be considered here. For simplicity we have considered that the efflux pumps depend on the concentration on one of the two sides of the membrane [29, 25]. However new results suggest that the transporter binding site for the molecule is inside the inner leaflet of the membrane [48]. If we think of the space inside the phospholipid bilayer as an additional volume with two permeable walls on either side the concentration in that volume would be in between those in the adjacent volumes.

3.2.1 Method application

The treatment starts with transforming the equations, now with the specific non-linearity, into the form given by (3.5),(3.6). The efflux terms (1.24) and (1.25) from chapter 1 suggest using K_M as the concentration rescaling term \mathcal{N} . On the other hand we will rescale the time to obtain dimensionless equations.

Thus we define $s = \frac{Cl_{CB}t}{V_B}$. Following above section the function $j(x)$ is given by:

$$j(x) = \gamma \frac{x}{1+x} \quad (3.22)$$

and γ is a parameter depending on the situation of the binding site. We find:

$$\gamma = -\frac{SV_M}{Cl_{CB}K_M} \frac{V_B}{V_C} \quad \text{intracellular binding} \quad (3.23)$$

and

$$\gamma = \frac{SV_M}{Cl_{CB}K_M} \frac{V_B}{V_A} \quad \text{extracellular binding} \quad (3.24)$$

Now the friction and force term are defined (eqs. 3.8). As we said before, the equilibrium concentration is found by finding the minimum in the potential. In the case of a Michealis-menten type flux the corresponding equation

$$\left. \frac{dV(x)}{dx} \right|_{x_{eq}} = -F(x_{eq}) = 0 \quad (3.25)$$

can be solved exactly, without the use of any approximation. The solution is:

$$x_{eq} = \frac{\alpha - \beta - \gamma a_{22} + \sqrt{4\alpha\beta + (\alpha - \beta - \gamma a_{22})^2}}{2\beta}. \quad (3.26)$$

Clearly the other saturation values can be derived through (3.6):

$$y_{eq} = -\frac{a_{21}x_{eq} + a_{23}}{a_{22}} \quad (3.27)$$

and using the conservation law to:

$$z_{eq} = \frac{Q_0}{V_z \mathcal{N}} - x_{eq} \frac{V_x}{V_z} - y_{eq} \frac{V_B}{V_z}. \quad (3.28)$$

Together with tables (3.1-3.4) all factors and constants are determined.

3.2.2 Comparison with experiment

We want to find out how good this approximation is. We will compare the result of our treatment with the numerical integration of the original system (eqs. 3.1-3.4), which does not contain approximations. A special showcase system is an absorption study of antibiotic CNV97100 [25]. In this study absorption of the antibiotic was investigated in Caco-2 cell cultures and four different models were considered. They differ in location of the efflux transporter (apical or basolateral membrane) and in location of the binding site (intra- or extracellular). Among these models the apical located pump with intracellular binding site was considered to be the model of best fit to the data. Thus,

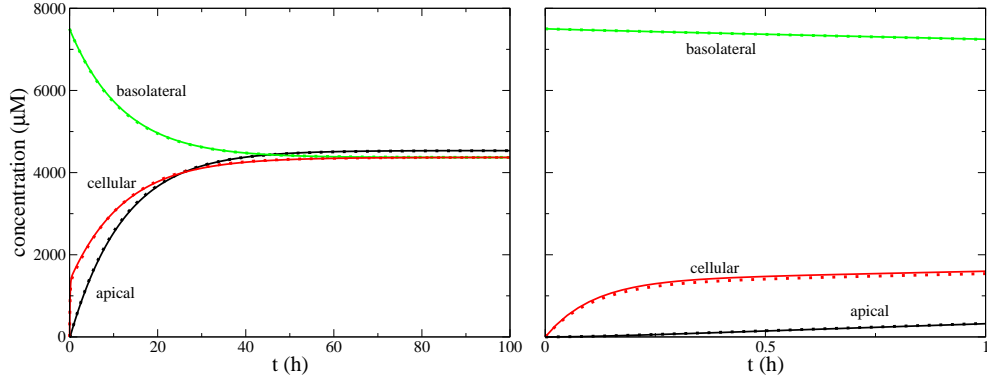


Figure 3.1: Time evolution of concentrations on either side of the cells and inside. *Dotted* line: Numerical integration of Eq. (3.1-3.4). *Continuous* line: explicit solution Eq.(3.16-3.18). Parameters taken from [25], intracellular binding site with MICHAELIS-MENTEN dynamics (1.24) is considered. Initial concentration $C_0 = 7500\mu M$ is applied on the basolateral side. *Right* graph: first hour amplified.

in the following we will focus on that case, however the other cases can be treated with the same method by changing the sign of V_M (efflux/influx) and interchanging compartments **A** with **B** or initial conditions (membrane where the pump is located). The form of binding site is chosen by the specific form of \mathcal{J} , here by the choice of γ to be either eq. (3.23) or eq. (3.24).

The parameters observed in mentioned study are summarised in table 3.5. Using these values one can compare the two solutions: the numerical integration and the approximated solution. Figures 3.1 and 3.2 show two different experimental situations, $7500\mu M$ loaded basolateral and $50\mu M$ loaded into the apical chamber. The first hour is amplified and one sees clearly the existence of time scales of different orders. One part of the process, the rapid absorption into the cellular compartment, is saturated after less than a quarter of an hour. Later the relaxation into the steady state is much slower and as we now from our analysis, governed by the sum of only two exponentials. Table 3.6 has all time scales and we see that $50\mu M$ loaded in the apical compartment yields time scales of 5 minutes on one hand and 14h and 24h on the other. Measurements at moments after a few minutes can be fitted to the sum of two exponentials rather than three. Besides we see that the measurements between 30 minutes and two hours are sufficiently far away from the discovered timescales, thus satisfying a linear consideration of the apparent permeability.

Coincidence of approximated with the numeric¹ solution is quite good. The thickness of the lines covers the differences between the two curves. We can conclude that at least under the studied circumstances the approximation is valid. If we now calculate the apparent permeabilities (eqs. 3.20 and 3.21)

¹For this numerical solution we have used a forth-order Runge-Kutta algorithm with a time step of 1s.

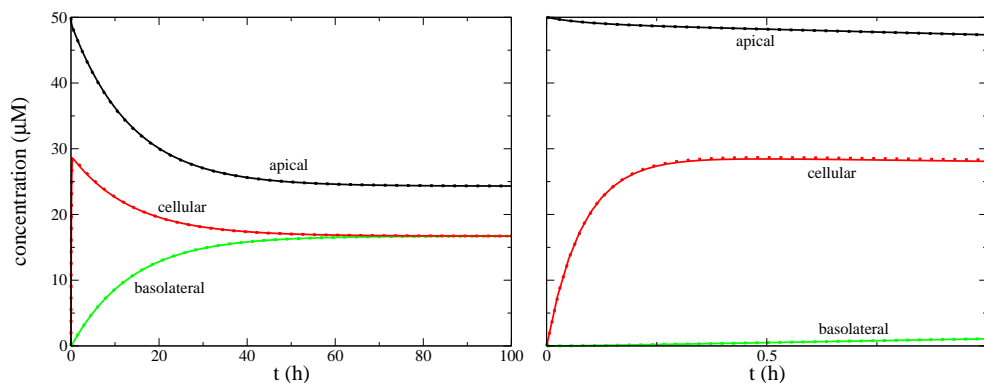


Figure 3.2: Same as figure 3.1, but initial concentration $50\mu M$ applied apically.

Table 3.5: Experimental parameters drawn from [25] used for the calculations.

Parameter	Measured Value
Cl_{AC}	$14.49 \times 10^{-5} cm^3/s$
Cl_{CB}	$3.528 \times 10^{-3} cm^3/s$
V_M	$6.17 \times 10^{-12} mol/(cm^2s)$
K_M	$0.376 mol/cm^3$
S	$4.2 cm^2$
V_A	$2 cm^3$
V_B	$3 cm^3$
V_C	$0.0738 cm^3$

we can compare our approximation with the experimental data. The numbers for the permeabilities are found in table 3.6 together with the quotient of both, called the *efflux ratio*. This value is of great significance for the experimentalist since it is a clear indicator for the presence of a (nonlinear) active absorption mechanism. In a purely passive absorption process it would not depend on initial concentration. Figures 3.3 compare the found values with the measurements of concentration on the receiving side. The lines drawn over the points correspond to their apparent permeability. When the drug initially is loaded into the apical chamber (top row) the coincidence is really good. In the case where the drug is loaded in the other (basolateral) chamber, one sees that the theory underestimates the pump's efficiency more and more the lower the amount of drug in the system is. This is not a consequence of our approximations as one can see in the graphs to the left. There we overlay the data once more with the numerical solution (dashed line) and since it underestimates the result in the same way, we conclude that the used Michaelis-Menten kinetics is insufficient to represent P-gp efflux at low initial concentrations when loaded basolaterally. Considerations of other pathways

Table 3.6: Time scales (when loaded apically) and apparent permeabilities predicted for different initial concentrations and different models (internal/external binding site).

C_0	binding	t_1	t_2	t_3	$P_{BA}^{app} \left(\frac{cm}{s} \right)$	$P_{AB}^{app} \left(\frac{cm}{s} \right)$	$\frac{P_{BA}^{app}}{P_{AB}^{app}}$
7500	int	12.3h	6.38min	23.6h	6.70×10^{-6}	6.37×10^{-6}	1.05
	ext	11.9h	6.67min	0.567h	6.80×10^{-6}	4.12×10^{-6}	1.65
5000	int	12.5h	6.27min	23.6h	6.73×10^{-6}	6.26×10^{-6}	1.07
	ext	11.9h	6.67min	0.567h	6.86×10^{-6}	3.97×10^{-6}	1.73
1000	int	13.5h	5.59min	23.6h	6.88×10^{-6}	5.57×10^{-6}	1.24
	ext	12.5h	6.70min	0.567h	7.18×10^{-6}	3.10×10^{-6}	2.32
50	int	13.8h	4.90min	23.6h	7.10×10^{-6}	4.88×10^{-6}	1.45
	ext	15.7h	6.73min	0.567h	6.94×10^{-6}	2.07×10^{-6}	3.35

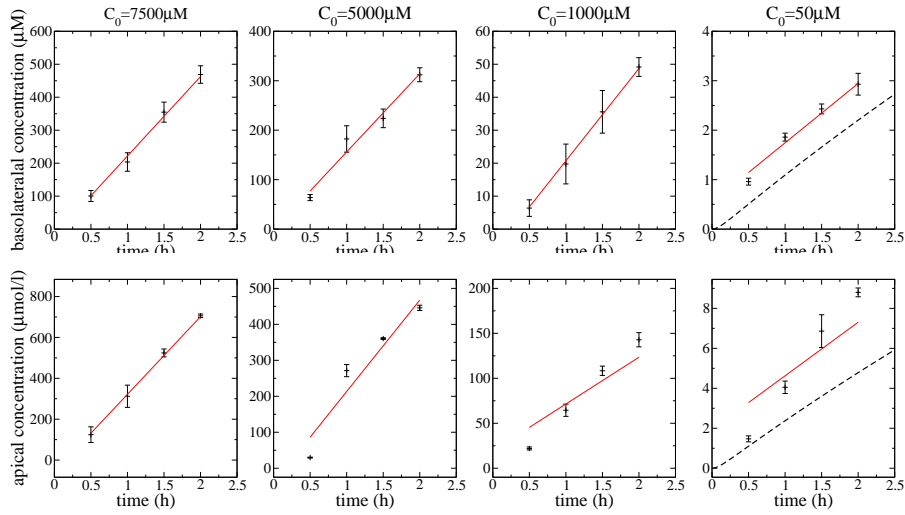


Figure 3.3: Antibiotic's concentration on the receiving side. (*Top*: drug loaded in apical compartment, *bottom*: basolateral loading.) Experimental values are from CNV97100 study. The *solid* line's slope is the prediction from the theoretical solution (shown in table 3.6) for intracellular binding, which was considered to be the model of best fit. The *dashed* line in the graphs on the right shows the numerical integration of the full system (3.1-3.4).

in the P-gp transporter protein are found in [49] and others.

3.2.3 Parameter dependence

One of the main points of our analysis is the ability to determine explicit expressions for the dependence of experimental quantities from the parameters of the system. Here lies one of the strengths of our solution: In figure 3.4 we plot the characteristic time scale for absorption t_1 , the equilibrium concentration ratio on both cell sides b_{eq}/a_{eq} and the efflux ratio $P_{BA}^{app}/P_{AB}^{app}$ as a function of the clearances Cl_{AC} and Cl_{CB} , the pump parameters V_M and K_M and the

initial concentration of drug C_0 . Analytic formulas give access to these results much easier than repetitive integration throughout parameter space plus extracting the data from the resulting trajectories.

Again, for simplicity, we limit our presentation to the case of a secretory pump located apically with intracellular binding site, the best model according to the analysis of [25]. As observed in fig. 3.4, an increase in the initial concentration C_0 implies a decrease in the characteristic time t_1 from a finite value to a minimum value, limiting t_1 to a range. Rising C_0 increases the equilibrium concentration ratio b_{eq}/a_{eq} . Although this ratio varies significantly, the steady concentration in the basolateral site, b_{eq} , shows a good linear dependence with C_0 (not shown in the figure). Note that the efflux ratio $P_{BA}^{app}/P_{AB}^{app}$ also decreases with increasing initial concentration, a feature supported by the experimental data, although the theoretical values deviate from the experimental results at low concentrations, a fact already discussed in the previous section. The clearance Cl_{CB} of the membrane where the pump is not situated has no influence on the equilibrium concentration and efflux ratios, but an increase of Cl_{CB} decreases the characteristic time t_1 , indicating a faster transport of the drug. On the other hand, an increase in the clearance Cl_{AC} of the cell membrane where the pump is located has the effect of decreasing the efflux ratio and increasing the equilibrium concentration ratio. For large initial concentrations, $C_0 = 7500\mu M$, the characteristic time t_1 shows an interesting behaviour with Cl_{AC} since it first increases and then decreases, indicating a very slow drug absorption for some intermediate values of the clearance.

At large concentrations, the three quantities analysed show a small dependence with respect to the pump parameters V_M and K_M , since the corresponding curves are almost flat. This makes it difficult to extract from the data accurate values of the pump parameters at those large concentrations. This suggests that lower concentrations would allow for a better experimental determination of the pump parameters - a practise used by experimentalists - but we have to take into account, as discussed above, that the accuracy of the model might worsen with decreasing concentration. In the graph, we have included negative values for V_M , which is equivalent to a change in the flow direction of the pump.

3.2.4 Error propagation

Apart from these considerations the analysis of parameter dependence is the first step towards examining the propagation of errors into the experimentally available quantities. For example it is clear from figure 3.4 (third and fourth column), that small differences in Cl_{AC} would be nearly unnoticed, due to the rather flat curve around its measured value (marked by the black arrow on top of the figures). On the other hand a small change in Cl_{CB} yields a big variation of time scale t_1 . We want to use an example to make this clear. Again we will

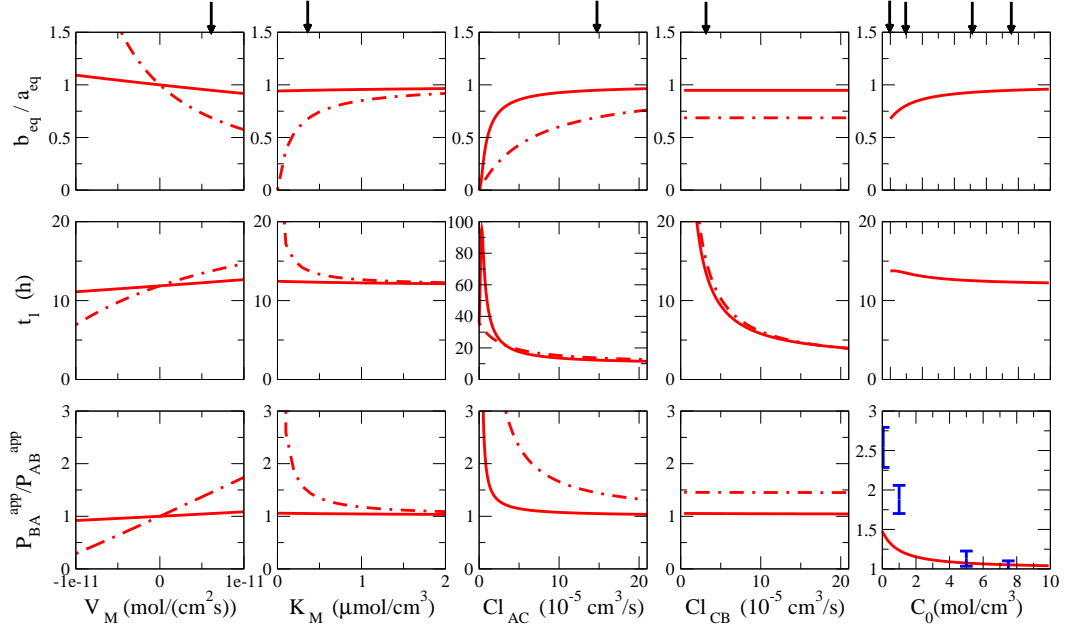


Figure 3.4: Secretory pump, intracellular binding site - *Top and middle:* equilibrium concentration ratio (basolateral/apical) and characteristic time (both for apical loading), *bottom:* efflux ratio $P_{BA}^{app}/P_{AB}^{app}$. Dependence on V_M and K_M (transporter parameters) and clearances Cl_{AC}/Cl_{CB} . *Continuous line:* $C_0 = 7500\mu M$, *dot-dashed line:* $C_0 = 50\mu M$. On the very right: dependence on initial concentration C_0 . Arrows on top mark the experimentally derived value. (Values for the respectively fixed parameters taken from table 3.5.)

use parameters derived in the CNV97100 absorption study and evaluate in which way a change in parameter influences the measurable quantities. This can be imagined as the variability in different sample cultures.

The distribution f_x of a value x in function of the distribution f_α of the parameter α is given by:

$$f_x(x) = f_\alpha(\alpha) \left| \frac{d\alpha(x)}{dx} \right|. \quad (3.29)$$

Knowing the distribution of value x , the mean value of x is defined by:

$$\langle x \rangle = \int_{x_1}^{x_2} x f_x(x) dx. \quad (3.30)$$

Alternatively, if this integration cannot be solved, one uses eq. (3.29) and writes:

$$\langle x \rangle = \int_{\alpha(x_1)}^{\alpha(x_2)} x(\alpha) f_\alpha(\alpha) d\alpha. \quad (3.31)$$

Correspondingly one finds:

$$\langle x^2 \rangle = \int_{x_1}^{x_2} x^2 f_x(x) dx \quad (3.32)$$

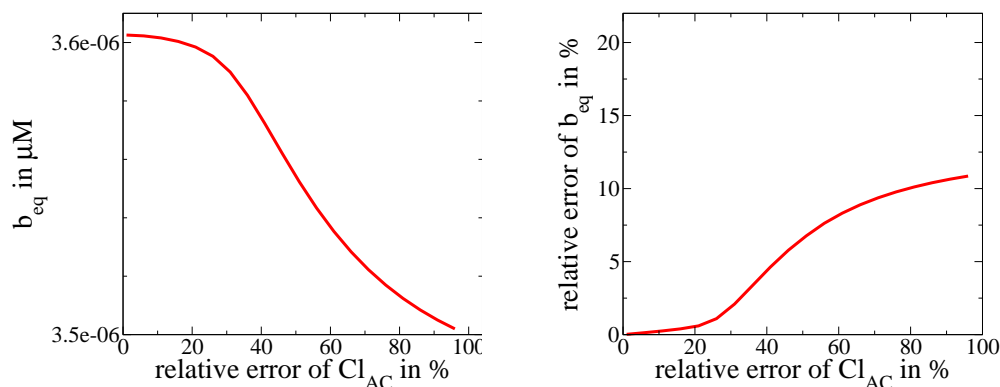


Figure 3.5: The mean basolateral concentration (*left*) and its relative error (*right*) in the case of $7500\mu M$ loaded apically, depending on the relative error of Cl_{AC} . A Gaussian distribution of clearance was assumed.

and the relative standard deviation

$$\sigma = \frac{\sqrt{\langle x^2 \rangle - \langle x \rangle^2}}{\langle x \rangle}. \quad (3.33)$$

Due to the nonlinearity it is not always easy to derive explicit expressions but having found the parameter dependencies before, above integrations are easily done numerically up to arbitrary precision.

Now we use the parameter set from [25] as done before. We chose an experimental set up (apical loading, $C_0 = 7500\mu M$) and the “model of best fit” (apical pump, intracellular binding) and can calculate for example the equilibrium concentration, or rather its distribution, on the receiving side. Figure 3.5 shows the mean value and the relative error versus the relative error of Cl_{AC} , the clearance of the apical membrane. Clearly one sees that the mean value itself is biased towards lower values by a (symmetric) error in the clearance. The relative error of the b_{eq} is a rising function with the remarkable feature of a range of very high slope. At a diversity in the clearance of about 30% the rise of the concentration’s error is much higher than for other values. How large the diversity of the cell membrane’s clearance is, is not the concern of this work but it allows to estimate the reasons for fluctuations in measurements.

3.3 Other nonlinearities and extensions of the model

The method we presented in section 3.1 to treat a three-compartment model and the proposed approximation are valid for a general form of nonlinear flux. We presented a solution for a specific form of flux known from enzyme dynamics in section 3.2. In the following we want to give a short analysis for

a different form of flux. Afterwards we suggest a possible extension of the model.

3.3.1 Michaelis-Menten with cellular retention

To account for the amount of drug which retains bound in the cell and is not available as substrate anymore, Korjamo et al. [50] used an additional constant K which rescales the intracellular concentration. In this case the dynamical equations (3.1-3.3) and the flux definition (1.24) become

$$\frac{dQ_A(t)}{dt} = +Cl_{AC} \left(\frac{Q_C}{V_C} \frac{1}{K} - \frac{Q_A}{V_A} \right) + \mathcal{J} \quad (3.34)$$

$$\frac{dQ_C(t)}{dt} = -Cl_{AC} \left(\frac{Q_C}{V_C} \frac{1}{K} - \frac{Q_A}{V_A} \right) - \mathcal{J} - Cl_{CB} \left(\frac{Q_C}{V_C} \frac{1}{K} - \frac{Q_B}{V_B} \right) \quad (3.35)$$

$$\frac{dQ_B(t)}{dt} = +Cl_{CB} \left(\frac{Q_C}{V_C} \frac{1}{K} - \frac{Q_B}{V_B} \right) \quad (3.36)$$

$$\mathcal{J} = \frac{SV_M \frac{Q_C}{V_C} \frac{1}{K}}{K_M + \frac{Q_C}{V_C} \frac{1}{K}} \quad (3.37)$$

When our transformation is applied to this system (here only intracellular binding is considered), the matrix element a_{21} is multiplied with a factor $1/K$ and the same factor rescales the parameter γ (eq. 3.23). With these changes the obtained results can be used. We will not go into much detail but the *efflux ratio* (ratio of (3.20) to (3.21)) as the value of main interest to the experimentalist has been calculated. For a parameter set as derived in the CNV97100 study one sees a lowering of the whole curve for rising retention (fig. 3.6). Retention of values smaller than one would raise the curve, but this is not reasonable. The curve does not change its shape much. We conclude that this extension of the three-compartment model is not good for fitting better to the experiment.

3.3.2 Outlook

The proposed method and approximation could be applied to many different systems. A consideration which might be of interest to pharmacology is an efflux \mathcal{J} of Hill type, $\frac{x^\alpha}{k^\alpha + x^\alpha}$, with exponents different α than 1. This formula is used to describe cooperative binding. Other possible fluxes could be analysed always if assumptions of a closed system with three compartments are fulfilled.

As an extension of this model one could overcome the coarse-grained picture of a cellular volume as one. It is known for example that P-gp expression is not the same along the intestinal wall. Spacial dependencies and diversity

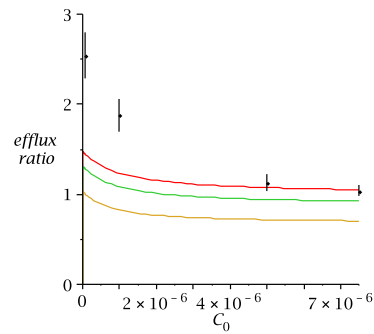


Figure 3.6: Efflux ratio versus initial concentration for different retention constants ($K = 1, 1.1, 1.3$, from top to bottom). The rest of parameters is taken from the CNV97100 experiment (section 3.2). $K = 1$ represents the case with no retention like in fig. 3.4, bottom, right. The experimental values are overlaid

in the amount of expressed transporter proteins could be added to the model. Assuming no horizontal transport (between the cells) one gets a row of similar equations, all coupled through the apical and basolateral volume. One could then expand the averaged dynamics around the mean value (similar to what was done in [51, 52]) and investigate the system with diverse parameters.

Chapter 4

Conclusions

We have analysed three different types of dynamical systems, all inspired by observations in biological systems.

The first presented system is a random walker in a plane, which correlates the direction of its steps with the one done before. It is thought to describe the motion of the zooplankton *Daphnia*, where such correlation between swim strokes were observed. The model predicts a linear growth of the averaged squared distance, after some time of transition. The angular correlation (2.4) determines both, the proportionality and the transition. For two distribution types these calculations were carried out explicitly: a sum of two delta peaks and a cut Gaussian. In the first case we could show that the position of the second peak, although accounting for only a tenth of the jumps, is crucial for the speed of diffusion. Different distributions could be investigated and the angular correlation can be drawn directly from experimental measured distributions. The presented results were published in [38].

In the same chapter we propose a simple model of food consumption. The food is a limited patch of diluted matter in a plane and does not grow again nor move in space. In the same plane there is other “matter” which diffuses freely along its gradient of concentration and additionally consumes the first matter. The consumption is proportional to the product of concentrations. We showed that under these circumstances a diffusion coefficient exists for which the uptaken food is maximal. Faster diffusion leads away from the food patch, slower diffusion means that one keeps too long on the same place and exhaust the provided food. These results, together with a mapping of the movement to the concept of an active Brownian particle, were published in [39].

In the subsequent part (chapter 3) we summarise a work on drug absorption. A model widely used in pharmacology for absorption studies has been examined. Being a mass conserving three-compartment model it has two degrees of freedom and we showed how to transform it into a problem of classical mechanics, a mass in a potential subjected to friction. Approximating the potential by a parabola and assuming the friction as a constant value taken at equilibrium, a closed form for the evolution of concentrations in the different

chambers has been given. The factors and constants in the solution depend on the specific form of the nonlinear flux. In the case of Michaelis-Menten flux the saturation concentration of the given model can be calculated exactly. Around this steady state the potential is expanded to second order. The resulting formulas are given. Furthermore the method was applied to an absorption experiment, done in the *Pharmaceutical Department* of the *University of Valencia*. Doing so we could validate the simplifications applied in the theoretical method, since the difference to the model used to fit the data is very small. Our results justify the linear assumption that was made in order to analyse the experimental data. The closed formulas of our approach allow to investigate how important the different parameters are on the experimental outcome and how an error or uncertainty in a parameter is propagated into the measurement. This might help to define experimental setups when new models are invented. In the last part we have shown how the proposed method is applied to another kind of nonlinear flux. The results are submitted to the *European Journal of Pharmaceutical Sciences* and available as a preprint version on an e-print server (arxiv.org).

Following the presented line of research within biological systems, a huge number of nonlinear systems or systems with many coupled subunits can be studied. One focus of further research lies in the circadian clocks, collections of neuronal cells acting as pacemakers for hormone release in mammals, whose phase is triggered by the natural change of light and darkness. Preliminary theoretical results reveal a constructive effect of cell's diversity for synchronisation with an external signal. For studying these systems a formerly developed method can be refined and be used for calculating approximate solutions. Validation of this refinement by applying it to known systems and usage on yet unknown systems will be another focus of future work. The expertise developed towards pharmacological processes might help to identify other systems in medical research, which permit the kind of treatment we have carried out concerning the active drug absorption.

Bibliography

- [1] A. Einstein, “On the movement of small particles suspended in stationary liquids be the molecular-kinetic theory of heat,” *Annalen der Physik*, vol. 17, pp. 549–560, 1905c.
- [2] M. v. Smoluchowski, “Zur kinetischen theorie der brownschen molekularbewegung und der suspensionen,” *Annalen der Physik*, vol. 21, pp. 756–780, 1906.
- [3] K. Pearson and J. Blakeman, *Mathematical contributions to the theory of evolution*, ch. XV. A mathematical theory of random migration. Dulau, London, 1906.
- [4] A. J. Lotka, *Elements of Physical Biology*. Baltimore: Williams and Wilkins Co., Inc., 1924.
- [5] V. Volterra, “Variazioni e fluttuazioni del numero d’individui in specie animali conviventi,” *Memor. Accad. Lincei., Ser. 6*, vol. 2, pp. 31–113, 1926.
- [6] W. O. Kermack and A. G. McKendrick, “A contribution to the mathematical theory of epidemics,” *Proc. Roy. Soc. Lond. A*, 1927.
- [7] E. M. Izhikevich, *Dynamical Systems in Neuroscience: The Geometry of Excitability and Bursting*. The MIT Press, 2007.
- [8] L. Gammaitoni, P. Hänggi, P. Jung, and F. Marchesoni, “Stochastic resonance,” *Reviews of Modern Physics*, vol. 70, no. 1, p. 223, 1998.
- [9] D. F. Russell, L. A. Wilkens, and F. Moss, “Use of behavioural stochastic resonance by paddle fish for feeding,” *Nature*, vol. 402, p. 291, 1999.
- [10] J. A. Freund, L. Schimansky-Geier, B. Beisner, A. Neiman, D. F. Russell, T. Yakusheva, and F. Moss, “Behavioral stochastic resonance: How the noise from a daphnia swarm enhances individual prey capture by juvenile paddlefish,” *Journal of theoretical Biology*, vol. 214, pp. 71–83, 2002.
- [11] M. Thattai and A. v. Oudenaarden, “Intrinsic noise in gene regulatory networks,” *PNAS*, vol. 98, no. 15, pp. 8614–8619, 2001.

- [12] P. H. Lu, L. Xun, and X. S. Xie, "Single-molecule enzymatic dynamics," *Science*, vol. 282, pp. 1877–1882, 1998.
- [13] W. Alt, "Modelling of motility in biological systems," *Iciam'87: Proceedings of the First International Conference on Industrial and Applied Mathematics*, 1987.
- [14] A. Okubo and S. A. Levin, *Diffusion and Ecological Problems: Modern Perspectives*. Springer-Verlag, 2nd ed., 2001.
- [15] A. Stevens, "A stochastic cellular automaton modeling gliding and aggregation of myxobacteria," *SIAM Journal of Applied Mathematics*, vol. 61, no. 1, pp. 172–182, 2000.
- [16] K. Pearson, "The problem of the random walk," *Nature*, vol. 72, p. 294, July 1905.
- [17] W. Ebeling, F. Schweitzer, and B. Tilch, "Active brownian particles with energy depots modeling animal mobility," *BioSystems*, vol. 49, pp. 17–29, 1999.
- [18] L. Michaelis and M. Menten, "Die kinetik der invertinwirkung," *Biochemische Zeitschrift*, pp. 333–369, 1913.
- [19] J. Hunter and B. H. Hirst, "Intestinal secretion of drugs. the role of p-glycoprotein and related drug efflux systems in limiting oral drug absorption," *Advanced Drug Delivery Reviews*, vol. 25, pp. 129–157, 1997.
- [20] P. V. Balimane, S. Chong, and r. A. Morrison, "Current methodologies used for evaluation of intestinal permeability and absorption," *Journal of Pharmacological and Toxicological Methods*, vol. 44, pp. 301–312, 2000.
- [21] P. Artursson and R. T. Borchardt, "Intestinal drug absorption and metabolism in cell cultures: Caco-2 and beyond," *Pharmaceutical Research*, vol. 14, no. 12, pp. 1655–1658, 1997.
- [22] J. D. Irvine, L. Takashi, K. Lockhart, J. Cheong, J. W. Tolan, H. E. Selick, and J. R. Grove, "Mdkc (madin-darby canine kidney) cells: A tool for membrane permeability screening," *Journal of Pharmaceutical Sciences*, vol. 88, no. 1, pp. 28–33, 1999.
- [23] P. Artursson, K. Palm, and K. Luthman, "Caco-2 monolayers in experimental and theoretical predictions of drug transport," *Advanced Drug Delivery Reviews*, vol. 46, pp. 27–43, 2001.
- [24] M. Holz and A. Fahr, "Compartment modeling," *Advanced Drug Delivery Research*, vol. 48, pp. 249–264, 2001.

- [25] I. Gonzalez-Alvarez, C. Fernandez-Teruel, T. Garrigues, V. Casabo, A. Ruiz-García, and M. Bermejo, “Kinetic modelling of passive transport and active efflux of a fluoroquinolone across caco-2 cells using a compartmental approach in nonmem,” *Xenobiotica*, pp. 1067–1088, December 2005.
- [26] Y. Raviv, H. Pollard, E. Bruggemann, I. Pastan, and M. Gottesman, “Photosensitized labeling of a functional multidrug transporter in living drug-resistant tumor cells,” *Journal of Biological Chemistry*, pp. 3975–3980, 1990.
- [27] M. D. Troutman and D. R. Thakker, “Efflux ratio cannot assess p-glycoprotein-mediated attenuation of absorptive transport: Asymmetric effect of p-glycoprotein on absorptive and secretory transport across caco-2 cell monolayers,” *Pharmaceutical Research*, vol. 20, pp. 1200–1209, August 2003.
- [28] M. D. Troutman and D. R. Thakker, “Novel experimental parameters to quantify the modulation of absorptive and secretory transport of compounds by p-glycoprotein in cell culture models of intestinal epithelium,” *Pharmaceutical Research*, vol. 20, pp. 1210–1224, August 2003.
- [29] A. Ruiz-García, H. Lin, J. M. Plá-Delfina, and M. Hu, “Kinetic characterization of secretory transport of a new ciprofloxacin derivative (cnv97100) across caco-2 cell monolayers,” *Journal of Pharmaceutical Sciences*, vol. 91, no. 12, pp. 2511–2519, 2002.
- [30] A. Ordemann, “Vortex-swarmling of the zooplankton daphnia,” *The Biological Physicist; The Newsletter of the Division of Biological Physics of the American Physical Society*, vol. 2, No. 3, pp. 5–10, August 2002.
- [31] A. Ordemann, G. Balaszi, and F. Moss, “Pattern formation and stochastic motion of the zooplankton daphnia in a light field,” *Physica A*, vol. 325, pp. 260–266, 2003.
- [32] U. Erdmann, W. Ebeling, L. Schimansky-Geier, A. Ordemann, and F. Moss, “Theory of active brownian particles: Application to experiments with swarms of the zooplankton daphnia,” *Journal of Theoretical Biology*, preprint 2003.
- [33] U. Erdmann, “Structure formation by active brownian particles with nonlinear friction,” in *Proceedings of the International Conference on Complex Systems* (Y. Bar-Yam, ed.), New England Complex Systems Institute, 1997.
- [34] U. Erdmann, W. Ebeling, F. Schweitzer, and L. Schimansky-Geier, “Brownian particles far from equilibrium,” *European Physical Journal B*, pp. 105–113, 2000.

- [35] U. Erdmann and W. Ebeling, "Collective motion of brownian particles with hydrodynamic interactions," *Fluctuation and Noise Letters*, 2003.
- [36] R. Wagner. a photo originally from wikipedia, changed by the author.
- [37] J. R. Strickler, "Observing free-swimming copepods mating," *Phil. Trans. R. Soc. Lond. B*, vol. 353, pp. 671–680, 1998.
- [38] N. Komin, U. Erdmann, and L. Schimansky-Geier, "Random walk theory applied to daphnia motion," *Fluctuation and Noise Letters*, 2004.
- [39] L. Schimansky-Geier, U. Erdmann, and N. Komin, "Advantages of hopping on a zig-zag course," *Physica A*, vol. 351, pp. 51–59, 2005.
- [40] P. M. Kareiva and N. Shigesada, "Analyzing insect movement as a correlated random walk," *Oecologia*, vol. 56, pp. 234–238, 1983.
- [41] M. Abramowitz and I. A. Stegun, eds., *Pocketbook of Mathematical Functions*. Verlag Harri Deutsch, 1984.
- [42] A. Fick, "Ueber diffusion," *Annalen der Physik*, vol. 170, p. 59, 1855.
- [43] W. E. Boyce and R. C. DiPrima, *Elementary Differential Equations and Boundary Value Problems*. John Wiley & Sons, Inc., 2001.
- [44] K. A. Lentz, J. W. Polli, S. A. Wring, J. E. Humphreys, and J. E. Polli, "Influence of passive permeability on apparent p-glycoprotein kinetics," *Pharmaceutical Research*, vol. 17, no. 12, 2000.
- [45] F. Faassen, G. Vogel, H. Spanings, and H. Vromans, "Caco-2 permeability, p-glycoprotein transport ratios and brain penetration of heterocyclic drugs," *International Journal of Pharmaceutics*, vol. 263, pp. 113–122, 2003.
- [46] P. V. Balimane, K. Patel, M. Anthony, and S. Chong, "Utility of 96 well caco-2 cell system for increased throughput of p-gp screening in drug discovery," *European Journal of Pharmaceutics and Biopharmaceutics*, vol. 58, pp. 99–105, 2004.
- [47] S. Yamashita, T. Furubayashi, M. Kataoka, T. Sakane, H. Sezaki, and H. Tokuda, "Optimized conditions for prediction of intestinal drug permeability using caco-2 cells," *European Journal of Pharmaceutical Sciences*, vol. 10, pp. 195–204, 2000.
- [48] M. Hennessy and J. Spiers, "A primer on the mechanics of p-glycoprotein the multidrug transporter," *Pharmacol Res*, doi:10.1016/j.phrs.2006.10.007, 2006.

- [49] P. Acharya, T. T. Thuy, J. W. Polli, A. Ayrton, H. Ellens, and J. Bentz, “P-glycoprotein (p-gp) expressed in a confluent monolayer of hmdr1-mdckii cells has more than one efflux pathway with cooperative binding sites,” *Biochemistry*, vol. 45, pp. 15505–15519, 2006.
- [50] T. Korjamo, H. Kemiläinen, A. T. Heikkinen, and J. Mönkkönen, “Decrease in intracellular concentration causes the shift in k_m value of efflux pump substrates,” *Drug Metabolism and Disposition*, vol. 35, no. 9, pp. 1574–1579, 2007.
- [51] S. de Monte, F. d’Ovidio, and E. Mosekilde, “Coherent regimes of globally coupled dynamical systems,” *Phys. Rev. Lett.*, vol. 90, no. 5, 2003.
- [52] S. de Monte, F. d’Ovidio, H. Chaté, and E. Mosekilde, “Effects of microscopic disorder on the collective dynamics of globally coupled maps,” *Physica D*, vol. 205, pp. 25–40, 2005.

Curriculum Vitae

Niko Komin

C/Morey 2, 2o

E-07001 Palma de Mallorca

niko@ifisc.uib-csic.es

+34 971 25 95 20

personal data

birth date and place: 15/08/1975, Berlin, Germany

nationality: German

academic education

since may 2005: PhD scholarship at the IFISC,
UIB-CSIC, Palma de Mallorca, ES

1997 - 2004: Physics studies at Humboldt University (HU) Berlin, DE
obtained degree: Diplom (Masters);
thesis title "*Active Motion of Biological Agents, taking the
Daphnia as an example*"

publications

2008: Komin, Toral: "*Drug absorption through a cell monolayer:
a theoretical work on a non-linear three-compartment mo-
del*" (submitted to European Journal of Pharmaceutical
Sciences)

2005: Schimansky-Geier, Komin, Erdmann: "*Advantages of Hop-
ping on a Zig-zag Course*"; (Physica A, 351:51-59, 2005)

2004: Komin, Erdmann, Schimansky-Geier: "*Random Walk The-
ory Applied to Daphnia Motion*"; (Fluctuation and Noise
Letters, 4(1):L151-L159, 2004)

oral communications

- 2008: “*Drug absorption in a three-compartment model*”,
- 4th BioSim conference, Budapest, HU
- “*Absorption of Drugs and Simplifications of Large, Diverse Systems*”,
- Cross-Disciplinary Physics Seminar at IFISC, Palma de Mallorca, ES
- 2007: “*A Theoretical Work on Efflux Transporters*”,
- Pharmacy Faculty, University of Valencia, ES
- 2006: “*Stochastic Effects in Drug Absorption*”,
- Cross-Disciplinary Physics Seminar at IMEDEA, Palma de Mallorca, ES
- BioSim Workshop Warwick, UK
- “*A short review of enzyme reactions*”,
- Seminar at Summer School “Physbio - Non-equilibrium Physics in Physics and in Biology”, St. Etienne, FR
- 2005: “*Motion of Biological Agents*”,
- Cross-Disciplinary Physics Seminar at IMEDEA, Palma de Mallorca, ES
- 2004: “*Motion of Biological Agents*”,
- Annual DPG Spring Conference, Regensburg, DE
- 2003: “*Random Walk theory applied to Daphnia motion*”,
- Seminar on occasion of Dr. A. Neiman’s visit to Berlin, DE
- 2001: “*Cellular Automata*”,
- Students’ Seminar at Humboldt University, Berlin, DE

poster communications

- 2008: “*Diversity in Large and Coupled Systems - (Gompertz Equation of Tumoral Growth)*”,
- FisEs08, Salamanca, ES
- 2007: “*Absorption of Pharmaceuticals Through Cell Monolayers*”,
- 3rd BioSim conference, Potsdam, DE
- workshop “From Complex Systems Theory to Clinical Neurology”, Dresden, DE
- “simCYP Hands-on Experience with Automated In Vitro-In Vivo Extrapolation - Applications”, Prague, CZ

“The role of light - dark cycle and constructive diversity in synchronizing circadian oscillators”,

- presented by Adrian Murza at EUFEPS Conference on Optimising Drug Development, Basel, CH

2006: *“An Intestinal Drug Transport Model”*

- Annual DPG Spring Conference, Dresden, DE

- Xarxa Temàtica “Dinàmicas no lineales de autoorganización espaciotemporal”, Barcelona, ES

“Nonlinear Transport of Molecules Through Cell Layers”,

- FisEs06, Granada, ES

“Absorption of Pharmaceuticals Through Cell Monolayers”,

- EUFEPS Conference on Optimising Drug Development, Basel, CH

2005: *A Hamiltonian formulation of a drug transport model* 1st

BioSim Conference, Palma de Mallorca, ES

PhD courses at the University of Balearic Islands

Métodos estocásticos de simulación. Dr. Raúl Toral and Pere Colet. 2006 [3 credits]

Fenómenos cooperativos y fenómenos críticos: aplicaciones. Dr. Maxi San Miguel, Dr. Tomas M. Sintes and Dr. Víctor Eguíluz. 2006 [3 credits]

Sistemas dinámicos no lineales y complejidad espacio-temporal. Dr. Maxi San Miguel, Dr. Emilio Hernández and Dr. Oreste Piro. 2006 [4 credits].

Fenómenos no lineales en Biología. Dr. Raúl Toral, Dr. Claudio Mirasso, Dr. Tomas Sintes and Dr. Oreste Piro. 2006 [4 credits].

Computación distribuida, Grid y E-ciencia. Dr. Joan Massó. 2006 [3 credits].

Workshops and Summer Schools

14/05-18/05 2007: *“simCYP Hands-on Experience with Automated In Vitro-In Vivo Extrapolation - Applications”*, Prague, CZ

04/06-08/06 2007: Workshop: *“From Complex Systems Theory to Clinical Neurology”*, Dresden, DE

13/08-8/10 2006: Summer School “*Physbio - Non-equilibrium in Physics and in Biology*”, St. Etienne, FR

08/08-12/08 2005: Summer School: “*Modelos matemticos en Biología: un viaje de ida y vuelta*”, Universidad Internacional de Andalucía, ES

Participation in Conferences

2008 “*Workshop on Dynamics and Evolution of Biological and Social Networks*”, Palma de Mallorca, ES

2005 “*The European Conference on Mathematical and Theoretical Biology*”, ECMTB 2005, Dresden, DE

Other skills

Programming (mainly) C/C++, Python, Maple

Office Applications Latex, Image Manipulation (GIMP), Office

Data Analysis gnuplot, grace, pylab

Languages German (native)

English (good)

Spanish (good)

Catalan (understanding medium, spoken basic)

Russian, Swedish, Arabic (some basic knowledge from earlier studies)

January 29, 2009